http://dx.doi.org/10.1016/j.istruc.2024.106776

Numerical investigation on post–fire resistance of cold–formed Q960 ultra high strength steel channel section stub columns

Xuanyi Xue[a,*], Tak-Ming Chan[a], Ben Young[a]

[a] *Department of Civil and Environmental Engineering, The Hong Kong Polytechnic University, Hong Kong, China*

Abstract

Numerical analyses on the residual resistant performance of cold–formed Q960 ultra high strength steel (UHSS) channel section stub columns after fire exposure were reported. The proposed numerical modelling method was validated by the existing experimental results of the cold–formed EN 1.4420 austenitic stainless steel, S690 high strength steel (HSS) and S960 UHSS channel section stub columns at room temperature, and the hot-rolled EN 1.4301 austenitic stainless steel channel section stub columns after exposure to fire, where the ultimate resistance, load–end shortening curve and failure mode were considered. The satisfactory comparisons demonstrate the appropriateness of the proposed numerical modelling methodology for the Q960 UHSS channel section stub columns after fire exposure. A parametric study considering different geometric dimensions and exposure temperatures was conducted, where a total of 410 numerical models were included. The geometric dimensions of cold–formed Q960 UHSS channel section stub columns changed the effects of exposure temperature on the load–end shortening curve. For the conditions after exposure temperature less than 600 °C, the slenderness limit of Class 3 in European code could be used for cold–formed Q960 UHSS channel section stub columns. When the exposure temperatures were at 700, 800 and 900 °C, the slenderness limit of Class 3 became unsuitable. The accuracy of design approaches in EN 1993-1-12, AISI S100, AS/NZS 4600 and direct strength method (DSM) was assessed. When the exposure temperatures were at 800 and 900 °C, there were noticeable differences between the numerical results

* Corresponding author.

E-mail address: xuexuanyi@126.com (X. Xue).

and results obtained from the abovementioned design approaches. The modification methods considering effects of exposure temperature and geometric dimensions were proposed for the EN 1993-1-12 design approach to predict ultimate resistance of the cold–formed Q960 UHSS channel section stub columns after different exposure temperatures.

Keywords:

Q960 ultra high strength steel; Channel section; Stub column; Ultimate resistance; Numerical analysis; Design recommendation.

1. Introduction

High strength steel (HSS) with yield strength larger than 460 MPa has been widely used in bridge and high–rise building structures [1]. Considering the advantages of high strength, the use of HSS reduces the steel plate thickness in component, which improves its fatigue performances and reduces welding difficulty [2]. Many investigations have been conducted to clarify the resistant performance of HSS components [3–5]. With the improvement of steel production technology, ultra high strength steel (UHSS) has gradually entered the vision of researchers and engineers. Even though the current application of UHSS on civil engineering structures was limited, the excellent strength properties make the UHSS have broad engineering application prospects. Compared with the HSS, the UHSS provides similar benefits. The benefits of UHSS are more obvious, because of better strength properties than the HSS. Some investigations have been conducted to clarify the resistant behaviours of the UHSS components. Wang et al. [2] studied the resistant performance of S960 UHSS angle and channel section stub columns, where experiments and numerical analyses were conducted. Shi et al. [6] performed experiments on the welded UHSS stub columns, where the effects of local buckling were clarified. Ma et al. [7] clarified the resistant performance of cold–formed

UHSS tubular sections, where a numerical modelling method including cold–forming effects on material properties was proposed. Li et al. [8] investigated the slenderness limits for the welded S960 UHSS columns. However, compared with the mild steel component, the investigations on the UHSS component are still very limited, which restricts the recommendation of UHSS design approaches and engineering applications. Fire caused significant negative impacts on the resistant performance of steel components, which is a common disaster for steel structures [9–11]. When a steel structure experienced fire without collapse, it is meaningful to evaluate whether it can be directly re-used, or requires repair or reconstruction [12–14]. Exposure temperatures change the microstructures of steels, which bring noteworthy effects on the residual mechanical properties [15–17]. Some investigations on the post–fire mechanical properties of different UHSSs have been conducted. Pandey and Young [18] conducted experiments on the residual monotonic stress–strain properties of the UHSS coupons from the cold–formed tubular members after exposure to fire. For the experiments conducted by Li and Young [19], the UHSS coupons from cold–formed square and rectangular hollow sections were used to reveal the effects of exposure temperatures on post–fire mechanical properties. The predictive methods for the key stress and strain properties were proposed, which balanced the predictive accuracy and convenience of engineering applications. Qiang et al. [20] clarified the post–fire mechanical properties of the S960 UHSS, where the effects of exposure temperatures were quantified. Xue et al. [21] studied the post–fire mechanical properties of the Q960 UHSS experimentally, where the different cooling methods were considered. Based on the abovementioned investigations, obvious changes were found in mechanical properties of the UHSS after exposure to elevated temperatures. Then, the effects of changes in the mechanical properties on the resistant performance of UHSS components after exposure to fire are worth investigating.

The post–fire resistant performances of different steel components have been studied by many scholars, where the experimental and numerical studies were conducted. Song

et al. [22] conducted the experiment on the restrained Q690 HSS column at post–fire condition. Su et al. [23] studied the residual resistance of the S960 UHSS welded I-section stub columns after exposure to elevated temperatures. Hua et al. [12] studied the post–fire shear resistance of the Q690 HSS plate girder though numerical analyses. Sagiroglu [24] performed the experimental study on the post–fire behavior of steel T–components. For the UHSS components, the relevant investigations are limited. Pandey and Young [25] studied the cold–formed S960 UHSS tubular joints experimentally, where the accuracy of current design approaches on residual strength of S960 UHSS tubular joints after exposure to fire was evaluated. Cho et al. [26] revealed the net section tension strength of bolted UHSS connections after exposure to fire through experiments and numerical simulations. The effects of exposure temperature on the load–bearing curve and failure mode of UHSS bolted connections were investigated. However, the residual resistant performance of cold–formed UHSS channel section stub columns after exposure to fire remained unclear.

To the best of the authors' knowledge, there are no reported test results on the residual resistant performance of the cold–formed UHSS channel section stub columns after exposure to fire. With the support of the experimental investigations on the post–fire mechanical properties of the Q960 UHSS [27,28], the numerical analysis could be used to study the residual resistant performance of the cold–formed Q960 UHSS channel section stub columns after exposure to fire. To solve the abovementioned issues, a series of numerical analyses on the cold–formed Q960 UHSS channel section stub columns were conducted in this study. In section 2 of this paper, a numerical modelling method including nonlinearity of material property and initial geometric imperfection was proposed to simulate the load–bearing performance of cold–formed Q960 UHSS channel section stub columns with different exposure temperatures. A parametric study consisting of 410 numerical models was conducted, where different geometric dimensions and exposure temperatures were included. In section 3 of this paper, the numerical results of the load–bearing curve, ultimate capacity and failure mode of the

cold–formed Q960 UHSS channel section stub columns with different exposure temperatures were discussed. In section 4 of this paper, the accuracy of design approaches in EN 1993-1-12 [29], AISI S100 [30], AS/NZS 4600 [31] and direct strength method (DSM) was assessed. A correction factor was suggested to quantify the post–fire ultimate resistance of cold–formed Q960 UHSS channel section stub columns. In general, channel section is one of the basic cross–sectional forms of cold–formed steel components. The results obtained from this study contribute to the formation of a comprehensive method for calculating the residual load–bearing performance of cold–formed UHSS structures after fire exposure.

2. Numerical investigation

2.1. Material model

To investigate the residual resistant performance of cold–formed Q960 UHSS channel section stub columns, the post–fire mechanical properties of the flat and corner Q960 UHSS need to be used in the numerical analysis as the material models. Based on the investigations [27,28], the post–fire mechanical properties of the flat and corner Q960 UHSS were obtained experimentally, as shown in Fig. 1, where the air–cooling treatment was selected. The air-cooling and water-cooling treatments were selected in many investigations on the post–fire mechanical properties of structural steels [19,25,32]. Compared with the air-cooling treatment, the water-cooling treatment performed the higher cooling rate. Hence, when the exposure temperature was relatively high, the carbon steels with water-cooling treatment usually performed the higher strength properties, compared with the carbon steels with air-cooling treatment. Similar conclusions were also observed in the investigations on the Q960 UHSS flat and corner coupon specimens [27,28]. To reveal the weakest resistance of the cold–formed Q960 UHSS channel section stub columns after fire, the air-cooling treatment was selected in this study. The locations of corner and flat coupon specimens were

shown in Fig. 2. The B_f, B_w, c, d, t and R_i denoted the outer flange width, outer web width, flat element width excluding the corner radius for flange, flat element width excluding the corner radius for web, wall thickness and inner corner radius, respectively. When the exposure temperature was lower than 600 °C, effects of elevated temperature exposure on the post–fire mechanical properties of the flat and corner Q960 UHSS were ignorable. With increment in the exposure temperature, the nonlinearity of the stress–strain curve changed, where the 700 °C was the turning point. Based on the experimental results in Ref. [27], the microstructure of the virgin Q960 UHSS consisted with the cementite and ferrite. For the virgin Q960 UHSS without fire exposure, the lattice dimension was relatively small, which enhanced the strength property. Austenitizing temperature of carbon steel is about 727 °C. When the exposure temperature was 700 °C, no austenite was formed in the Q960 UHSS. However, the lattice dimension increased because of the heat treatment, which reduced the strength property. Hence, the strength properties of the Q960 UHSS after exposure to 600 and 700 °C were lower than those of the virgin Q960 UHSS without fire exposure. When 800 and 900 °C exposure temperatures were applied, austenite was formed in the Q960 UHSS. Then, the granular pearlite was formed after cooling treatment. Therefore, the strength properties of the Q960 UHSS after exposure to 800 and 900 °C were higher than those of the Q960 UHSS after exposure to 700 °C. When the exposure temperature was at 900 °C, the more thorough austenitization would be achieved in the Q960 UHSS, compared with 800 °C exposure temperature. This should bring beneficial effects on the formation of granular pearlite. Hence, the strength properties of the Q960 UHSS after 900 °C exposure temperature were higher than those of the Q960 UHSS after 800 °C exposure temperature. It is worth noting that the experimental results on the Q960 UHSS flat and corner coupon specimens performed the similar variation trends. Similar conclusions were observed in the experimental research in Ref. [33], which proved the reliability of the experimental results. Hence, to clarify the residual resistant performance of cold–formed Q960 UHSS channel section stub columns, the monotonic

stress–strain properties of the virgin specimens and the specimens after 600 ~ 900 °C elevated temperatures were considered in the numerical analysis. The true stress–strain curves of the flat and corner Q960 UHSS were introduced into corresponding areas of the numerical model, as shown in Fig. 3.

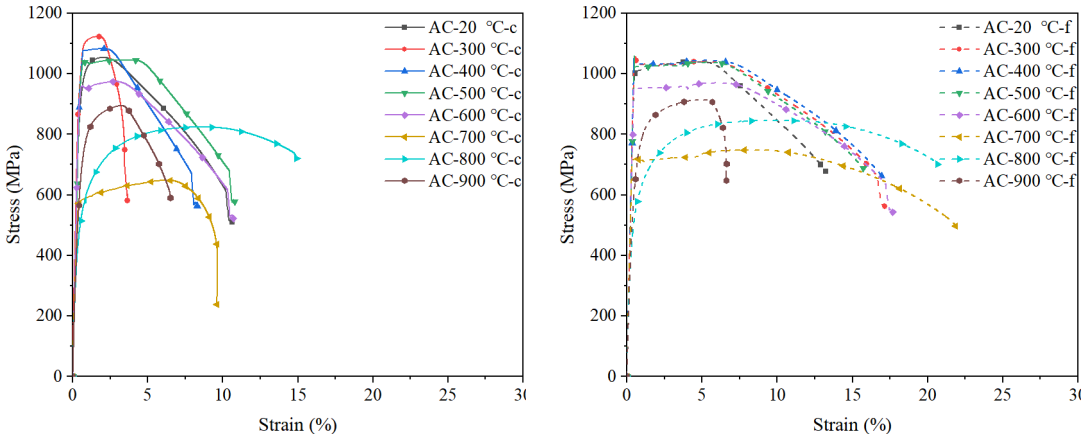

Fig. 1. Monotonic stress–strain curves of the Q960 UHSSs: (a) corner area; (b) flat area [27,28].

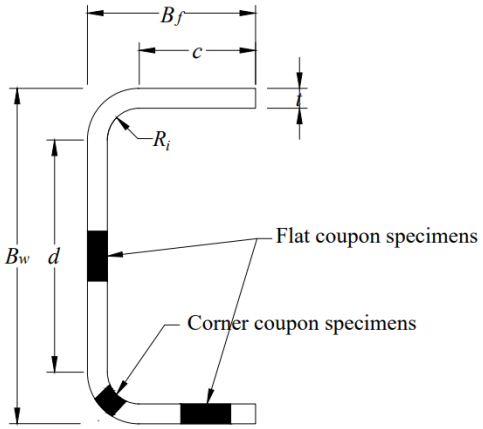

Fig. 2. locations of corner and flat coupon specimens.

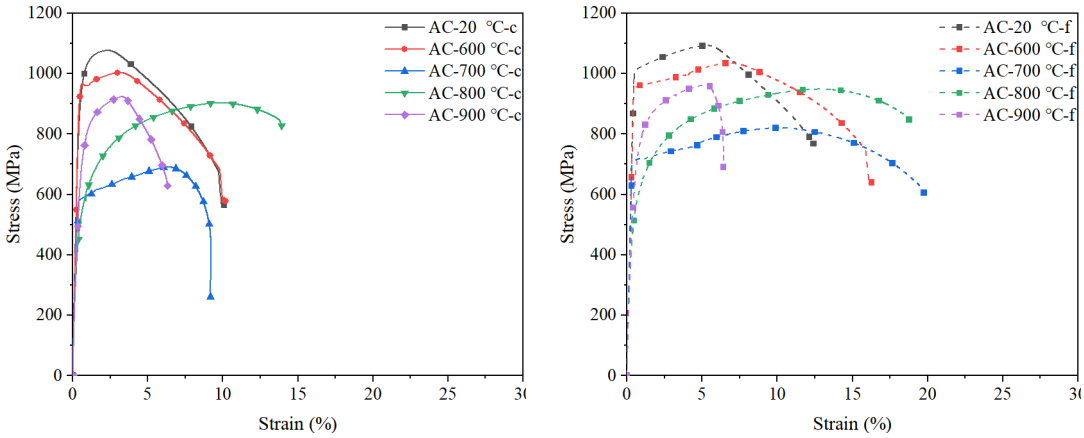

Fig. 3. True stress–strain curves of Q960 UHSSs: (a) corner area; (b) flat area [27].

2.2. Numerical modelling method

The numerical analysis in this study was conducted in the finite element (FE) software ABAQUS [34] The S4R shell element was used to build the cold–formed Q960 UHSS channel section stub column, which was recommended in many investigations on cold–formed components [2,3,35]. In order to balance the calculation consumption and accuracy, a convergence study was conducted to determine the appropriate element size, where different element sizes ranging from 0.2t to 2t were considered. The square shell element was used in the numerical analysis, where the side length was considered to be the element size. After convergence study, the element size was determined to be equal to the thickness of cold–formed section t, which was also recommended in Refs [2,3]. For the boundary condition, two concentric reference points were built in the numerical model (Fig. 4), which were coupled with the upper and bottom end sections respectively. The translation and rotation degrees of freedom of one of the reference points were restrained. The other reference point only released the longitudinal translation degree of freedom. To consider the effects of initial geometric imperfections on the resistant performance of cold–formed Q960 UHSS channel section stub columns, two steps were conducted in the numerical analysis. For the first step, the elastic buckling analysis on the numerical model without the initial geometric imperfection was performed. Then, the eigenvalue buckling modes were obtained. The first buckling mode was considered

to be the distribution form of the initial geometric imperfection, whose amplitude was determined to be $t/10$. Based on the numerical analyses in References [2,3], $t/10$ was validated to be the appropriate amplitude of the initial geometric imperfection for the cold–formed S690 HSS and S960 UHSS channel section stub columns. After that, the effects of the initial geometric imperfection could be introduced in the second step. For the second step, the static Riks analysis considering the geometric and material nonlinearities was conducted to clarify the resistant performance of the cold–formed Q960 UHSS channel section stub column. It is worth noting that the value of membrane residual stress was clearly lower than that of bending residual stress. Hence, the effects of membrane residual stress were not included in the numerical analysis, which was also suggested in References [2,3]. The effects of bending residual stress were reflected in the tensile test of the corner and flat coupon. Therefore, the material model in the Section 2.1 included the effects of the bending residual stress. Based on the above discussion, it is believed to be appropriate to ignore the effects of the membrane and bending residual stresses in the numerical analysis, which was recommended by many researchers [2,3,35].

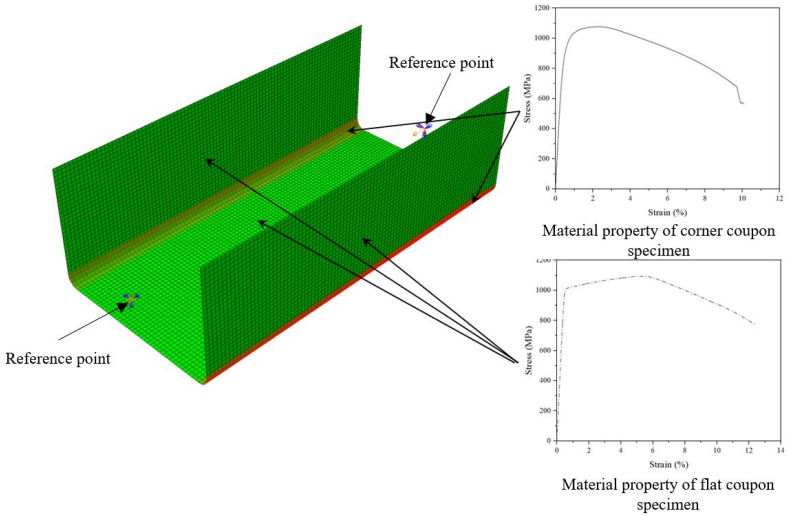

Fig. 4. Numerical model of the cold–formed Q960 UHSS channel section stub column [27].

2.3. Validation on numerical simulation

To validate the accuracy of the numerical modelling method, some experimental results on the cold–formed EN 1.4420 austenitic stainless steel [36]/ S690 HSS [3]/ S960 UHSS [2] channel section stub columns under room temperature were selected. The monotonic stress–strain properties of the EN 1.4420 austenitic stainless, the S690 HSS and the S960 UHSS under room temperature were similar to those of the post–fire stress–strain properties of the flat and corner Q960 UHSS introduced in Section 2.1. The same specimen ID was remained in this study for better traceability. The comparisons in the load–end shortening curve between numerical and experimental results were shown in Fig. 5. A good agreement was observed in the load–end shortening curves from the experiment and numerical analysis. The comparisons in the ultimate resistance were shown in Table 1. The mean value and coefficient of variation (COV) of the $N_{u,FE}/N_{u,test}$ were 1.045 and 0.040 respectively. The $N_{u,FE}$ and $N_{u,test}$ denoted the ultimate load from numerical analysis and experimental test, respectively. The failure mode of test specimens could also be predicted by the numerical analysis effectively (Fig. 6). The unit of the deformation magnitude in Fig. 6 was in mm. For the post–fire condition, the experiment on the hot-rolled EN 1.4301 austenitic stainless steel channel section stub columns after exposure to fire in Ref. [37] was selected to validate the numerical modelling method in this study. The load–end shortening curves of the numerical analysis in this study agreed well with those of experimental results in Ref. [37]. The experimental results of the ultimate resistance for the 14 specimens in Ref. [37] were used to validate the accuracy of the numerical modelling method, as shown in Table 2. The mean value and coefficient of variation (COV) of the $N_{u,FE}/N_{u,test}$ were 1.028 and 0.026 respectively. The comparison in failure mode of the numerical model was also similar to that of the experimental specimen in Ref. [37], as shown in Fig. 8. The unit of the deformation magnitude in Fig. 8 was mm. This study mainly focused on the effects of changes in mechanical properties of the Q960 UHSS after elevated temperature on the ultimate resistance of the cold–formed Q960 UHSS

channel section stub columns. The validation as mentioned earlier also included the stub column experiments on the post–fire condition, which stated the accuracy of the numerical modelling method. Hence, it is considered that the *t*/10 was the appropriate value for the geometric imperfection amplitude for the cold–formed Q960 UHSS channel section stub columns. Based on the above discussion, the numerical modelling method in this study could be used to predict the resistant performance of the cold–formed Q960 UHSS channel section stub column after elevated temperature properly. It is worth noting that only the cold–formed steel components were considered in the validation. In order to expand the applicability of numerical simulation, it should be considered to complete the verification of welded steel components in the future.

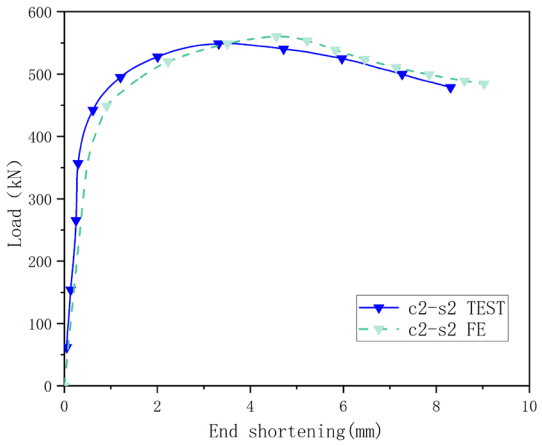

(a)

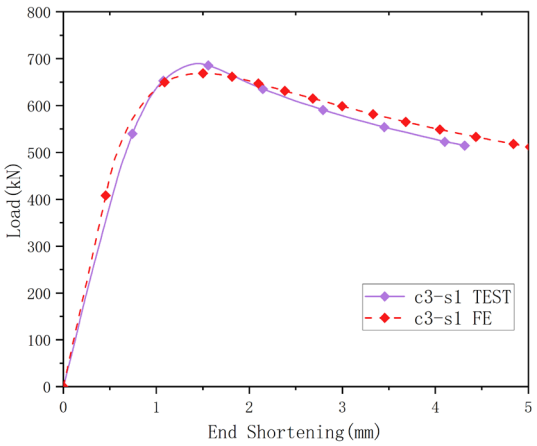

(b)

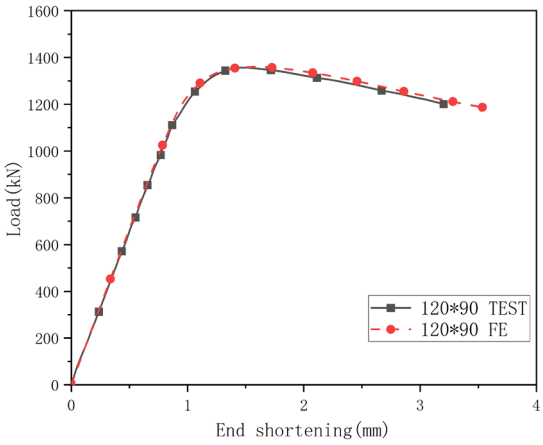

(c)

Fig. 5. Comparison in load–end shortening curve between numerical and experimental results under room temperature: (a) EN 1.4420 austenitic stainless steel [36]; (b) S690 HSS [3]; (c) S960 UHSS [2].

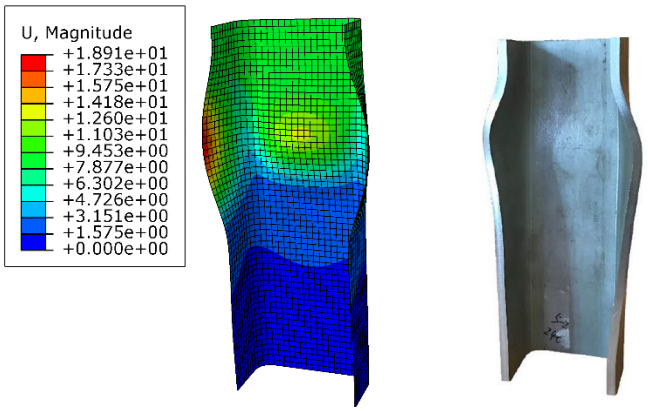

(a)

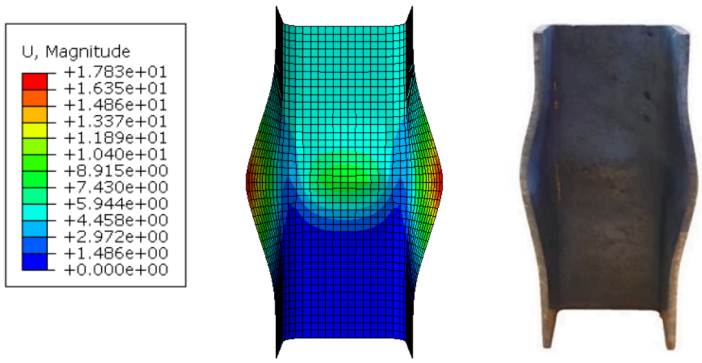

(b)

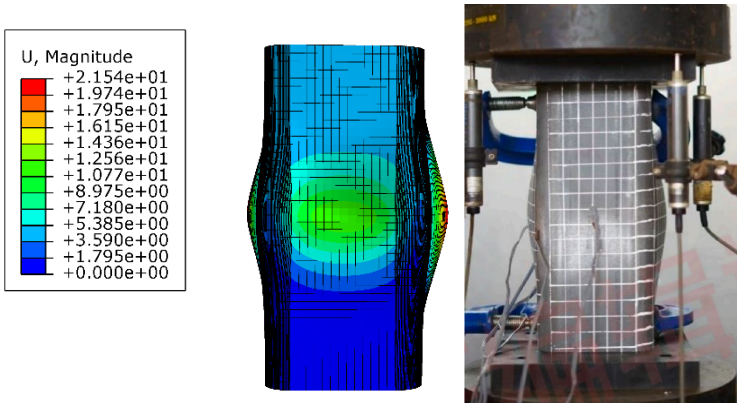

(c)

Fig. 6. Failure modes of the numerical model and experimental specimen under room temperature: (a) EN 1.4420 austenitic stainless steel [36]; (b) S690 HSS [3]; (c) S960 UHSS [2].

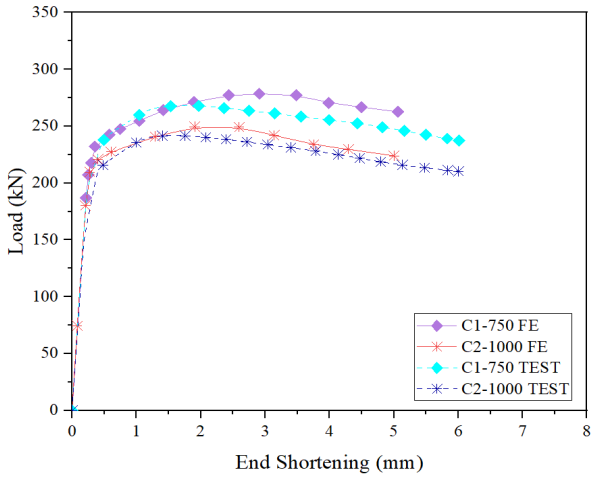

Fig. 7. Comparison in load–end shortening curve of hot-rolled EN 1.4301 austenitic stainless steel channel section stub columns between numerical and experimental results under post–fire condition [37].

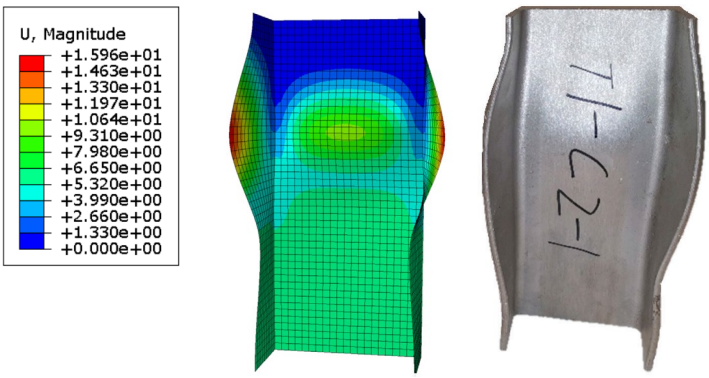

Fig. 8. Failure modes of the numerical model and experimental specimen [37] under post–fire condition.

Table 1

Comparison in ultimate resistances of cold–formed EN 1.4420 austenitic stainless steel [36], S690 HSS [3] and S960 UHSS [2] channel section stub columns between experimental and numerical results under room temperature.

Material	Specimen ID	$N_{u,FE}/N_{u,test}$
EN 1.4420 austenitic stainless steel	C1-S1	1.075
	C1-S2	1.073
	C2-S1	1.024
	C2-S2	1.027
S690 HSS	C4-S2	1.032
	C6-S1	1.005
	C6-S2	0.987
	C8-S1	0.997
	C3-S1	0.969
S960 UHSS	C80-45-6	1.132
	C100-45-6	1.073
	C120-45-6	1.087
	C80-55-6	1.065
	C100-60-6	1.033
	C120-70-6	1.035
	C120-90-6	1.097
	C120-90-6-R	1.056
	Mean	1.045
	COV	0.040

Table 2

Comparison in ultimate resistances of hot-rolled EN 1.4301 austenitic stainless steel channel section stub columns [37] between experimental and numerical results under post–fire condition.

Material	Specimen ID	$N_{u,FE}/N_{u,test}$
EN 1.4301 austenitic stainless steel	C1-30	1.040
	C1-300	1.041
	C1-450	1.045
	C1-600	1.051
	C1-750	1.039
	C1-850	1.039
	C1-1000	1.032
	C2-30	1.015
	C2-300	0.994
	C2-450	1.039
	C2-600	0.982
	C2-750	0.966

	C2-850	1.053
	C2-1000	1.052
	Mean	1.028
	COV	0.026

2.4. Parametric study

There were differences in the mechanical properties between the corner and flat areas of the cold–formed Q960 UHSS channel section stub column. To include the effects of the ratio between corner area to flat area, the two different outer web widths (150 mm and 270 mm) were considered, which was similar to those in Ref. [2]. The outer flange widths were determined by the aspect ratio of the channel section stub column. The aspect ratio was the ratio between the outer web width to outer flange width. In this parametric study, the aspect ratios were 1.0, 1.5, 2.0, 2.5 and 3.0, which were recommended in Ref. [3]. The wall thickness changed from 2 mm to 26 mm, which ensured that the Class 1, 2, 3, and 4 cross–sections were considered in this parametric study. The above classes of cross-sections were defined in EN 1993-1-1 [38]. After the cold–forming process, the differences in mechanical properties between the flat and corner Q960 UHSS were observed, which was caused by the cold–forming process. The above differences were influenced by the inner corner radius to wall thickness ratio. The mechanical property of the Q960 UHSS used in this study was obtained from the specimens with inner corner radius to wall thickness ratio 1.6. To simulate the same cold–forming effects, the inner corner radius to wall thickness ratios of all numerical models were controlled to be 1.6. The details of cross–section geometric dimensions of the cold–formed Q960 UHSS channel section stub columns were shown in Table 3. The length was selected to be $1.25(B_f + B_w)$. The amplitude of the initial geometric imperfection was determined to be 0.1 wall thickness. Considering the post–fire mechanical properties of the flat and corner flat and corner Q960 UHSS, five different material models were introduced in the numerical model respectively, which were from the virgin specimens and the specimens after 600 ~ 900 °C elevated temperatures as

296 detailed in Ref. [27]. Therefore, a total of 410 numerical models were included in the
297 parametric study. The interactions among these key parameters could be revealed
298 through the 410 numerical models in this study. Based on the parametric study results,
299 the modification design methods considering the interactions among these key
300 parameters were proposed.
301
302 Table 3
303 Cross–section geometric dimensions selected for parametric study.

B_w (mm)	B_f (mm)	t (mm)	R_i (mm)
150	50	2, 4, 6, 8, 10	3.2, 6.4, 9.6, 12.8, 16
	60	2, 4, 6, 8, 10, 12	3.2, 6.4, 9.6, 12.8, 16, 19.2
	75	4, 6, 8, 10, 12, 14	6.4, 9.6, 12.8, 16, 19.2, 22.4
	100	4, 6, 8, 10, 12, 14, 16, 18	6.4, 9.6, 12.8, 16, 19.2, 22.4, 25.6, 28.8
	150	6, 8, 10, 12, 14, 16, 18, 20, 22, 24	9.6, 12.8, 16, 19.2, 22.4, 25.6, 28.8, 32, 35.2, 38.4
270	90	4, 6, 8, 10, 12, 14, 16, 18	6.4, 9.6, 12.8, 16, 19.2, 22.4, 25.6, 28.8
	108	4, 6, 8, 10, 12, 14, 16, 18, 20	6.4, 9.6, 12.8, 16, 19.2, 22.4, 25.6, 28.8, 32
	135	6, 8, 10, 12, 14, 16, 18, 20, 22, 24	9.6, 12.8, 16, 19.2, 22.4, 25.6, 28.8, 32, 35.2, 38.4
	180	6, 8, 10, 12, 14, 16, 18, 20, 22, 24, 26	9.6, 12.8, 16, 19.2, 22.4, 25.6, 28.8, 32, 35.2, 38.4, 41.6
	270	10, 12, 14, 16, 18, 20, 22, 24, 26	16, 19.2, 22.4, 25.6, 28.8, 32, 35.2, 38.4, 41.6

304 Note: B_w denoted the outer web width, B_f denoted the outer flange width, t denoted the wall thickness, R_i
305 denoted the inner corner radius. Inner corner radius to wall thickness ratio was fixed at 1.6.

306 3. Results and discussions

307 3.1. Load–end shortening curve and failure mode

308 The exposure temperature changed the monotonic stress–strain curves of the Q960
309 UHSS, which brought differences in the load–end shortening curves of the channel
310 section stub columns. However, effects of the exposure temperature on the load–end

311 shortening curve were influenced by the geometric dimensions of cold–formed Q960
312 UHSS channel section stub column. Two different numerical models were selected to
313 reveal this issue, which were the C 150 × 60 × 12 and C 270 × 180 × 6, as shown in
314 Fig. 9. The label "C 150 × 50 × 12" indicated that the outer web width was 150 mm,
315 the outer flange width was 50 mm and the wall thickness was 12 mm. The C 150 × 50
316 × 12 and C 270 × 180 × 6 were Class 1 (stocky) and Class 4 (slender), respectively. For
317 the load–end shortening curve of the C 150 × 60 × 12 without fire exposure (Fig. 9a),
318 there was a platform segment after the initial segment. When the exposure temperatures
319 were at 600 and 700 °C, the nonlinearity of load–end shortening curve was similar to
320 that of the component without fire exposure, which was caused by the similar
321 monotonic stress–strain curves in Fig. 1. When the exposure temperatures were at 800
322 and 900 °C, there was a noteworthy increment in the load after the initial rising segment,
323 because of the beneficial effects of the strain hardening in monotonic stress–strain
324 curves in Fig. 1. In this regard, the nonlinearity of load–end shortening curve of the
325 cold–formed Q960 UHSS channel section stub column with 800 and 900 °C exposure
326 temperature was similar to that of cold–formed stainless steel column [39]. Considering
327 the cross–section of C 150 × 60 × 12 which was Class 1 (stocky), adverse effects of
328 buckling on load–bearing performance were relatively limited. Then, after the yield
329 strength of material on cross–section of C 150 × 60 × 12 was achieved, the stress could
330 continue to increase, which resulted in the increment in load resistance. Therefore, the
331 strain hardening in monotonic stress–strain curves brought beneficial effects on the
332 load–bearing performance of C 150 × 60 × 12 model. The nonlinearity of monotonic
333 stress–strain curve could be reflected to the load–end shortening curve. The C 270 ×
334 180 × 6 was Class 4 (slender), which was more prone to buckling. For the C 270 × 180
335 × 6 without the fire exposure, the descending segment was observed after the initial
336 rising segment. The nonlinearity of load–end shortening curves with 600 and 700 °C
337 was similar with that of the load–end shortening curve without fire exposure. When the
338 exposure temperatures were at 800 and 900 °C, the increment in load after the initial

rising segment was also observed. However, the aforementioned increment in load after the initial rising segment of the C 270 × 180 × 6 was clearly smaller than that of the C 150 × 50 × 12. The buckling in C 270 × 180 × 6 weakened the beneficial effect of the strain hardening on load–bearing performance. When the exposure temperatures were at 800 and 900 °C, the initial resistant stiffness of C 150 × 60 × 12 and C 270 × 180 × 6 reduced, which was caused by the reductions in elastic modulus of the corner and flat Q960 UHSSs.

In general, the geometric dimensions of cold–formed Q960 UHSS channel section stub columns changed the effects of the exposure temperature on the load–end shortening curves. The coupling effects of geometric dimensions and stress–strain properties on the load–bearing performance of the cold–formed Q960 UHSS channel section stub columns after fire exposure should be concerned. Failure modes corresponding to the ultimate limit state were collected, where Fig. 10a and b were obtained from C 150 × 60 × 12 model and Fig. 10c and d were obtained from C 270 × 180 × 6 model. The unit of the deformation magnitude in Fig. 10 was mm. It is easy to see that even though the exposure temperatures were different, the deformation distribution form barley changed. Local buckling was also observed in the web and flange, which was similar to failure mode as described in Section 2.3 of this paper. This proved that numerical modelling method was appropriate for the cold–formed Q960 UHSS channel section stub column. It is believed that the effects of exposure temperature on the failure modes of the cold–formed Q960 UHSS channel section stub columns could be ignored. The results could further confirm the similarity in numerical modelling method between the room temperature condition and post–fire condition.

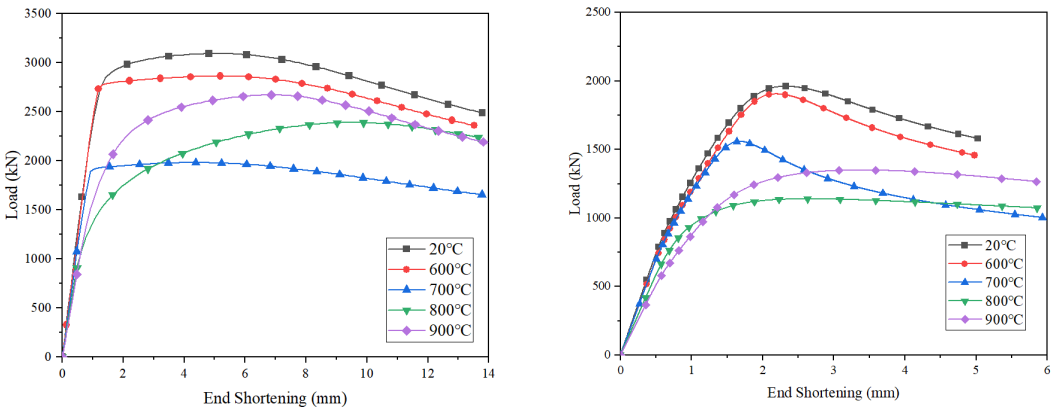

362 Fig. 9. Load–end shortening curves of cold–formed Q960 UHSS channel section stub
363 column: (a) C 150 × 50 × 12; (b) C 270 × 180 × 6.

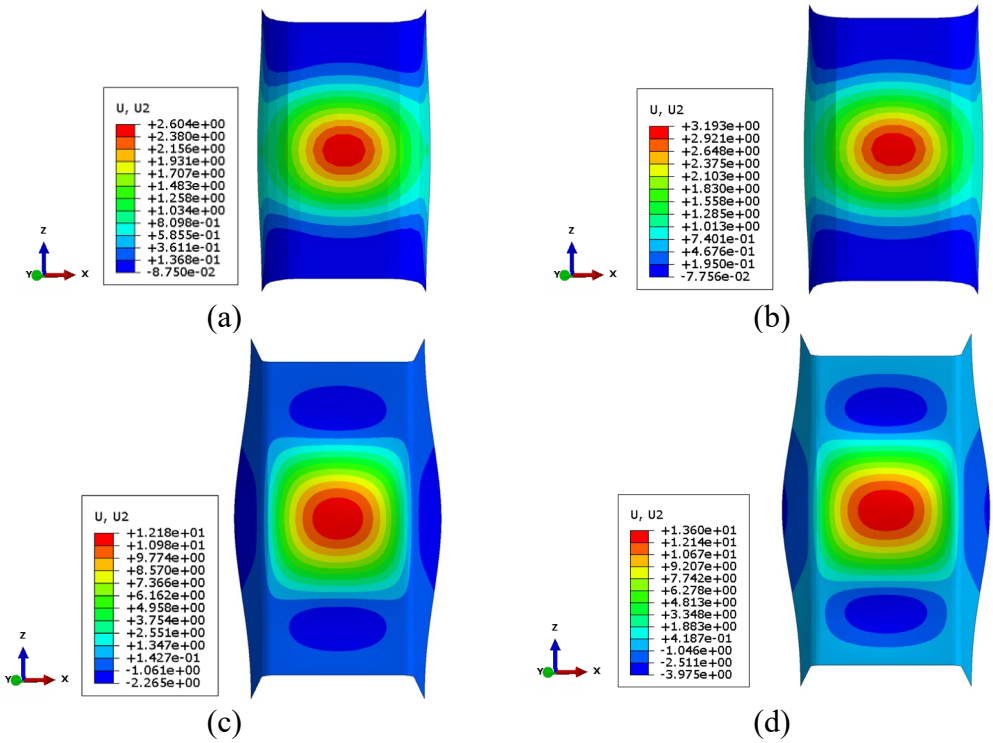

364 Fig. 10. Failure modes of cold–formed Q960 UHSS channel section stub column: (a)
365 C 150 × 60 × 12 and 20 °C; (b) C 150 × 60 × 12 and 700 °C; (c) C 270 × 180 × 6 and
366 800 °C; (d) C 270 × 180 × 6 and 900 °C.

367 3.2. Ultimate capacity

368 After the FE parametric study, the ultimate resistance of cold–formed Q960 UHSS
369 channel section stub columns with different geometric dimensions and exposure
370 temperatures were obtained, as shown in Fig. 11. The length of the cold–formed corner

was controlled by wall thickness, where the inner corner radius to wall thickness ratio was fixed at 1.6. Hence, considering the structural form of the channel section stub columns, the length to thickness ratio of cross–section $(2c+d)/t$ was selected to quantify the cross–section slenderness. In general, with increment in $(2c+d)/t$, the N_u/A decreased gradually. The N_u and A denoted the ultimate load from parametric study and gross cross–section area. The effects of exposure temperature on the ultimate resistance changed, with increment in $(2c+d)/t$. When the $(2c+d)/t$ was relatively small, the stub columns with 700 °C exposure temperature performed the lowest N_u/A. The reason was that when the $(2c+d)/t$ was relatively small, adverse effects from buckling were limited. The strain hardening in the corner and flat Q960 UHSSs brought beneficial effects on the N_u/A. The smaller $(2c+d)/t$, the higher the utilization rate of material strength property by the cold–formed Q960 UHSS channel section stub columns. Then, the N_u/A was controlled by the f_u of the corner and flat Q960 UHSSs to a certain extent. f_u denoted the ultimate strength. The corner and flat Q960 UHSSs with the 700 °C exposure temperature performed the lowest f_u, which reduced the N_u/A correspondingly. With increment in $(2c+d)/t$, adverse effects of the buckling became severer. Therefore, beneficial effects of strain hardening in the corner and flat Q960 UHSSs disappeared gradually. The N_u/A was mainly influenced by the f_y of the corner and flat Q960 UHSSs. f_y denoted the yield strength. When the exposure temperature was 800 °C, the lowest f_y was observed. Hence, the stub columns with 800 °C exposure temperature performed the lowest N_u/A. When the $(2c+d)/t$ was larger than 20, the cold–formed Q960 UHSS channel section stub column with 800 °C performed the lowest N_u/A. For cold–formed Q960 UHSS channel section stub column with 700 and 900 °C, the turning point of $(2c+d)/t$ was about 35.

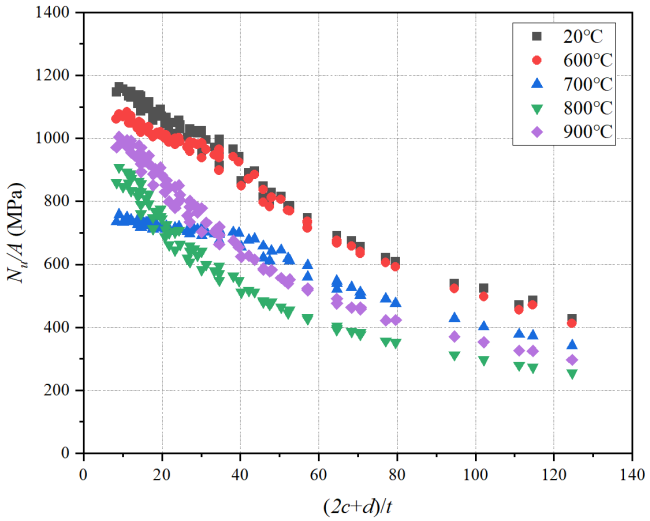

Fig. 11. N_u/A variation trends of cold–formed Q960 UHSS channel section stub columns after different exposure temperatures.

4. Evaluation and design recommendation

4.1. Evaluation of current design approaches

4.1.1. European design code

In EN 1993-1-12 [29], the design approaches of components with steel grades ranging from S460 to S700 were introduced. For the stub column, the cross–sections were divided into four classes, which was determined by the $c/t\varepsilon$ of most slender plate element. The material coefficient $\varepsilon = (235/f_y)^{0.5}$. For the channel section, the c was the width of flat element excluding the corner radius. For the Class 1, 2 and 3, the yield loads Af_y could be achieved. The Class 4 failed before the yield loads Af_y because of the local buckling. Considering that the f_u was not included in the design approach, the beneficial effects of strain hardening on the load–bearing capacity of the stub columns were not included in EN 1993-1-12 [29]. For the structural steel with the clear yield plateau, the above design approach was appropriate. However, the above design approach might be not appropriate when there was no yield plateau in the stress–strain curve but obvious strain hardening existed. The Class 3 slenderness limit in EC3 was

assessed in this study. Aspect ratio of the cold–formed Q960 UHSS channel section stub columns was controlled between 1 and 3 in this study. Then, compared with the internal web, the outstand flange performed the worse buckling resistance. The overall class of cross–section was determined by the outstand flange class. The slenderness limit of Class 3 in EC3 was shown in Fig. 12, where $c/t\varepsilon$ = 14. The $c/t\varepsilon$ of the outstand flange was used to conduct the assessment. For the N_u/Af_y, the mechanical properties of the flat Q960 UHSS with different exposure temperatures were selected. For the virgin cold–formed Q960 UHSS channel section stub columns without fire exposure, the $c/t\varepsilon$ could basically meet the requirement in EC3 for the slenderness limit of Class 3. When the exposure temperature was 600 °C, the scatter distribution was similar to that of stub columns without fire exposure. When the exposure temperatures were at 700, 800 and 900 °C, the slenderness limit of Class 3 in EC3 became unsuitable.

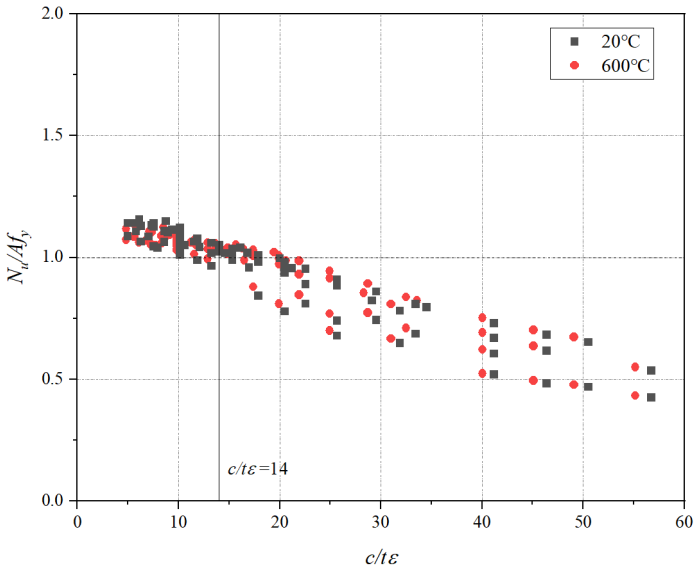

(a)

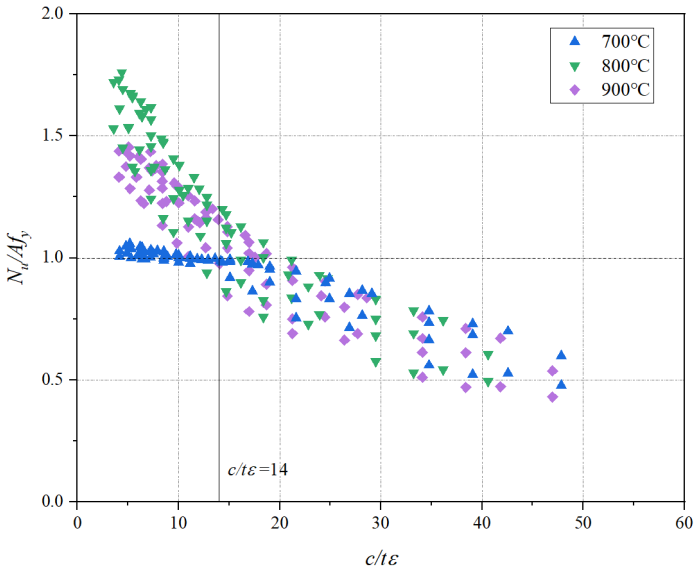

(b)

Fig. 12. Assessment of Class 3 slenderness limit in EC3 of channel sections in compression: (a) for 20 and 600 °C and (b) for 700, 800 and 900 °C.

For the design approach in EC3 [29], the ultimate resistance of Class 4 was $A_{eff}f_y$, where the A_{eff} was the effective cross–section area. The Eqs. (1) and (2) were used to determine the effective width c_{eff} of the Class 4 cross–section for the outstand and internal plate elements respectively. The Eq. (3) was used to determine the local slenderness $\bar{\lambda}_p$ of plate element. For the outstand and internal plate elements of uniformly compressed component, the values of buckling factor k_σ were 0.43 and 4.0 respectively. The end stress ratio ψ was 1 for the uniformly compressed condition. Then, the comparison in the ultimate resistance between the numerical results and results from design approach in EC3 was conducted (Fig. 13). For the virgin cold–formed Q960 UHSS channel section stub columns without fire exposure, the numerical results N_u were basically larger than those from EC3 design approach N_{EC3}. The mean value and COV of the N_u/N_{EC3} for the virgin cold–formed Q960 UHSS channel section stub columns without fire exposure were 1.11 and 0.05 respectively. To quantify the accuracy of EC3 design approach, the mean value and COV of N_u/N_{EC3} of the cold–formed Q960 UHSS channel section stub columns with different exposure temperatures were collected, as shown in

Table 4. When the exposure temperatures were at 800 and 900 °C, the accuracy of design approach in EC3 on the ultimate resistance of cold–formed Q960 UHSS channel section stub columns was reduced. When the exposure temperatures were at 600 and 700 °C, the distribution form of the N_u/N_{EC3} scatter points was similar to that of condition without elevated temperature exposure. When the exposure temperatures were at 800 and 900 °C, the values of N_u/N_{EC3} were significantly larger than 1.00, when the c/t was smaller than 7.50. The above differences for the 800 and 900 °C exposure temperatures were caused by the strain hardening in the stress–strain curves. Based on the stress–strain properties in Section 2.1, the noteworthy strain hardening was observed in the Q960 UHSS after exposure to 800 and 900 °C. Furthermore, there was no yield plateau in the stress–strain curves of the Q960 UHSS after exposure to 800 and 900 °C. Therefore, the stress of the cold–formed Q960 UHSS channel section stub columns with Class 1, 2 and 3 could continue to increase from f_y to f_u, when the exposure temperatures were at 800 and 900 °C. The above increment in stress brought beneficial effects on the N_u. However, the beneficial effects from the strain hardening on the N_u were not included in EC3 [29]. Then, the EC3 design approach was significantly conservative, when the c/t was relatively small. After that, with increment in the c/t, the accuracy of the EC3 design approach on the N_u of the cold–formed Q960 UHSS channel section stub columns with 800 and 900 °C exposure temperatures was improved. For the cold–formed Q960 UHSS channel section stub columns with Class 4, the buckling prevented the increment in stress from f_y to f_u. Therefore, even though the beneficial effects from the strain hardening on the N_u were not included in EC3 [29], the design approach still performed the good accuracy, when the c/t was larger than 7.50.

$$c_{eff}=\left(\frac{1}{\bar{\lambda}_p}-\frac{0.055(3+\psi)}{\bar{\lambda}_p^2}\right)c\leq c \quad \text{for} \quad \bar{\lambda}_p\geq 0.673 \tag{1}$$

$$c_{eff}=\left(\frac{1}{\bar{\lambda}_p}-\frac{0.188}{\bar{\lambda}_p^2}\right)c\leq c \quad \text{for} \quad \bar{\lambda}_p\geq 0.748 \tag{2}$$

$$\bar{\lambda}_p = \sqrt{\frac{f_y}{f_{cr}}} = \frac{c/t}{28.4\varepsilon\sqrt{k_\sigma}} \quad (3)$$

468

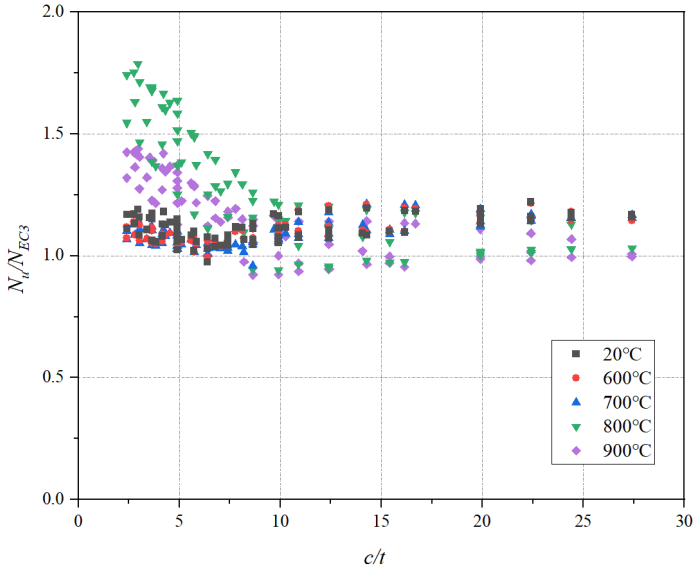

469

470 Fig. 13. Comparisons between the FE results and results from EC3 design approach.

471 Table 4

472 Comparisons between FE and predicted results from different design approaches.

Exposure temperatures	N_u/N_{EC3}		N_u/N_{DSM}		N_u/N_{AISI}	
	Mean	COV	Mean	COV	Mean	COV
20 °C	1.11	0.05	1.12	0.08	1.15	0.04
600 °C	1.10	0.04	1.12	0.09	1.15	0.04
700 °C	1.09	0.05	1.10	0.08	1.13	0.04
800 °C	1.30	0.19	1.33	0.17	1.36	0.17
900 °C	1.16	0.13	1.22	0.11	1.26	0.10

473

474 **4.1.2. North American specification and Australian/New Zealand standard**

475 The assessment on the North American Specification AISI S100 [30] and
476 Australian/New Zealand standard AS/NZS 4600 [31] was conducted in this section. The
477 nominal axial strengths N_{nl} of the channel section stub column under concentrical
478 compressive loading was determined by the Eq. (4). The design failure stresses f_n was
479 determined by the Eq. (5), which considered the coupling effects of global and local
480 buckling. The slenderness factor $\lambda_c = (f_y/f_{cre})^{0.5}$, where the f_{cre} was the lowest results of

481 the elastic flexural, torsional and flexural–torsional buckling stresses of the components.
482 The effective width c_{eff} of the outstand and internal plate elements was calculated by
483 the Eq. (6), where the $\lambda=(f_y/f_{cr})^{0.5}$. For the channel section stub column, the c was the
484 flat element width excluding the corner radius. Based on the above statement, the
485 beneficial effects of strain hardening on the load–bearing capacity of the stub columns
486 were not included in the design approach in AISI S100 [30] and AS/NZS 4600 [31],
487 which was similar to the design approach in EN 1993-1-12 [29]. When there was a yield
488 plateau in the stress–strain curve of the structural steel, the above design approaches
489 could be accurate. However, for the Q960 UHSS after exposure to 800 and 900 °C, the
490 obvious strain hardening was observed. The beneficial effects from the strain hardening
491 on ultimate resistance of the cold–formed Q960 UHSS channel section stub columns
492 were not considered in the design approach in AISI S100 [30] and AS/NZS 4600 [31].
493 Hence, the applicability of the design approach in AISI S100 [30] and AS/NZS 4600
494 [31] to N_u of the cold–formed Q960 UHSS channel section stub columns after exposure
495 to 800 and 900 °C was still worth the further evaluation. The comparisons in ultimate
496 resistance between FE results and results from AISI S100 were shown in Fig. 14. When
497 no exposure temperature was applied, the ultimate resistance could be predicted by AISI
498 S100 accurately. The mean value and COV of N_u/N_{AISI} for the cold–formed Q960 UHSS
499 channel section stub columns with different exposure temperatures were shown in Table
500 4. When the exposure temperatures were at 600 and 700 °C, the predictions of ultimate
501 resistance from AISI S100 [30] and AS/NZS 4600 [31] were basically accurate, which
502 were similar to those of virgin cold–formed Q960 UHSS channel section stub columns
503 without fire exposure. When the exposure temperatures were at 800 and 900 °C, the
504 design approaches in AISI S100 [30] and AS/NZS 4600 [31] were too conservative to
505 be directly used in the prediction of ultimate resistance of cold–formed Q960 UHSS
506 channel section stub columns after fire exposure. It is clear to see when the c/t was
507 smaller than 10.00, the ultimate resistance of cold–formed Q960 UHSS channel section
508 stub columns with 800 and 900 °C exposure temperatures were obviously

underestimated by the AISI S100 [30] and AS/NZS 4600 [31]. After that, when the *c*/*t* was larger than 10.00, the relatively good accuracy was observed in the ultimate resistance prediction of design approaches in the AISI S100 [30] and AS/NZS 4600 [31]. The above phenomenon of AISI S100 [30] and AS/NZS 4600 [31] was similar to that of EC3 [29].

$$N_{nl} = A_{eff} f_n \tag{4}$$

$$f_n = \begin{cases} \left(0.658^{\lambda_c^2}\right) f_y & \text{for} \quad \lambda_c \leq 1.5 \\ \left(\frac{0.877}{\lambda_c^2}\right) f_y & \text{for} \quad \lambda_c > 1.5 \end{cases} \tag{5}$$

$$c_{eff} = \left(\frac{1}{\lambda} - \frac{0.22}{\lambda}\right) c \leq c \tag{6}$$

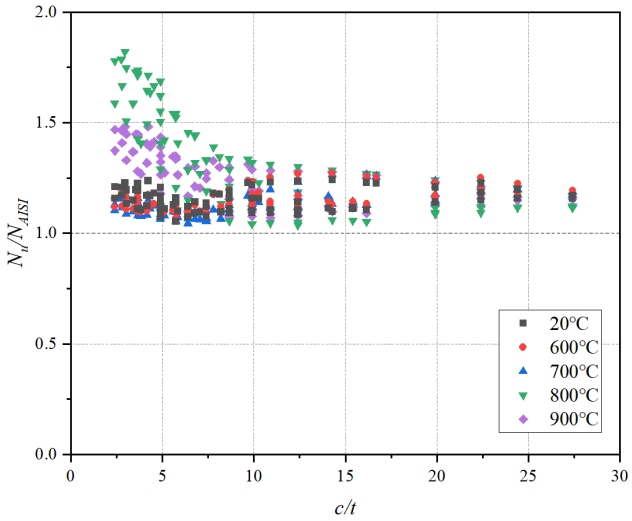

Fig. 14. Comparisons between the FE results and results from AISI S100.

4.1.3. Direct strength method

The DSM was proposed to overcome the complex calculation process in effective width method, especially for the cold–formed steel components with complex cross–sectional form [40]. The design equation of DSM was shown as Eq. (7). The slenderness factor of local buckling $\lambda_l = (f_y/f_{crl})^{0.5}$, where f_{crl} was the smallest local buckling stress of plate elements in cross–section. The DSM in AISI S100 [30] was applicable to the cold–formed steel components with material yield strength lower than 655 MPa. Then, the

applicability of the DSM on the ultimate resistance of the cold–formed Q960 UHSS channel section stub columns after exposure to different exposure temperatures was evaluated in this study. For the prediction on the ultimate resistance of the cold–formed Q960 UHSS channel section stub columns, the f_y was used in the DSM, rather than the f_u. Hence, the beneficial effects from the strain hardening on ultimate resistance of the cold–formed Q960 UHSS channel section stub columns were ignored. Therefore, the N_u of the cold–formed Q960 UHSS channel section stub columns after exposure to 800 and 900 °C might be underestimated by DSM, when the c/t was relatively small. The comparisons in ultimate resistance between FE results and results from DSM were shown in Fig. 15. The mean value and COV of N_u/N_{DSM} for the cold–formed Q960 UHSS channel section stub columns with different exposure temperatures were shown in Table 4. When the c/t was relatively small, the DSM could be used to predict the ultimate resistance of the virgin cold–formed Q960 UHSS channel section stub columns without fire exposure. With increment in c/t, the accuracy of DSM on ultimate resistance of the virgin cold–formed Q960 UHSS channel section stub columns was reduced. When the exposure temperatures were at 600 and 700 °C, the distribution form of N_u/N_{DSM} scatter points was similar to that of condition without elevated temperature exposure. When the exposure temperatures were at 800 and 900 °C, the DSM performed the obvious reduction in accuracy on the residual ultimate resistance of the cold–formed Q960 UHSS channel section stub columns, especially when the c/t was smaller than 10.00.

$$N_{DSM}=\begin{cases} Af_y & \text{for} \quad \lambda_l \le 0.776 \\ \left(1-\dfrac{0.877}{\lambda_l^{0.8}}\right)\dfrac{1}{\lambda_l^{0.8}}Af_y & \text{for} \quad \lambda_l > 0.776 \end{cases} \tag{7}$$

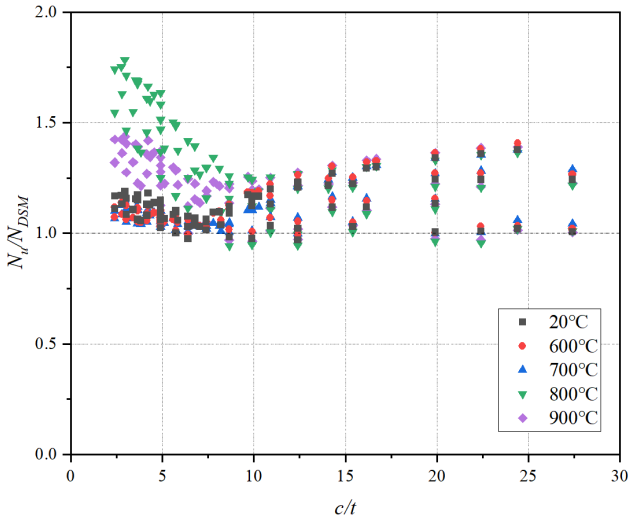

Fig. 15. Comparisons between the FE results and results from DSM.

4.2. Modification design method

Changes in stress-strain properties of the Q960 UHSS after exposure to elevated temperatures were observed in the Refs. [27,28]. The changes in stress-strain properties brought noteworthy effects on the resistant performance of the cold–formed Q960 UHSS channel section stub columns. To evaluate the residual resistant performance of the cold–formed Q960 UHSS structures, it is necessary to predict the post–fire ultimate resistance of the cold–formed Q960 UHSS channel section stub columns. Based on the discussion in section 4.1 of this paper, the design approach in EN 1993-1-12 [29] could accurately predict the ultimate resistance of the virgin cold–formed Q960 UHSS channel section stub columns without fire exposure. However, the prediction accuracy of design approach in EC3 [29] on the cold–formed Q960 UHSS channel section stub columns after different exposure temperatures could be improved. Hence, the EC3 design approach was selected for modification in this study. Two proposals were introduced in this subsection. It is worth noting that the resistant mechanism of cold–formed Q960 UHSS channel section stub columns after elevated temperature was not changed. The reduction in accuracy was caused by the changes in stress–strain properties of the Q960 UHSS after exposure to elevated temperature. To determine the post-fire mechanical properties of structural steels, the curve fitting method was used

in many Refs. [41–43]. Hence, for the modification proposal I, to quantify the effects of post–fire mechanical properties of the Q960 UHSS on the ultimate resistance of the cold–formed Q960 UHSS channel section stub columns, the curve fitting method was also selected in this study. For the modification proposal II, the negative relations between the N_u/N_{EC3} and $(2c+d)/t$ were observed through the graphic evaluation. The above negative relation was selected to improve the accuracy of the design approach in EC3 [29] on the ultimate resistance of the cold–formed Q960 UHSS channel section stub columns after exposure to elevated temperatures.

4.2.1. Modification proposal I

A correction factor $\eta = N_{u,T}/N_{EC3,20}$ for the design approach in EC3 [29] was proposed, where the $N_{u,T}$ was the ultimate resistance after exposure to T °C from the numerical analysis and the $N_{EC3,20}$ was the ultimate resistance without the fire exposure calculated by the design approach in EC3 [29]. Based on the numerical results in subsection 3.2 of this paper and the EC3 design approaches in subsection 4.1.1, the values of η for cold–formed Q960 UHSS channel section stub columns with different exposure temperatures could be obtained. Then, after the numerical fitting, the Eq. (8) was suggested to predict the η of the cold–formed Q960 UHSS channel section stub columns with different exposure temperatures, where the coefficients were shown in Table 5. The comparison in correction factor η between FE results and results from Eq. (8) was shown in Fig. 16. The mean value and COV of $\eta/\eta_{predicted}$ for the cold–formed Q960 UHSS channel section stub columns with 600, 700, 800 and 900 °C were shown in Table 6. It is clear to see that the Eq. (8) could be used to predict the correction factor η of the cold–formed Q960 UHSS channel section stub columns with different exposure temperatures accurately. The comparisons between numerical results and results calculated by Eq. (8) and EC3 design approaches were shown in Fig. 17. Compared with the current design approaches introduced in subsection 4.1, the correction factor proposed for the design approach in EC3 [29] performed the better accuracy on the

prediction of the ultimate resistance of the cold–formed Q960 UHSS channel section stub columns after fire exposure, especially when the exposure temperatures were at 800 and 900 °C.

$$\eta=\frac{A_1-A_2}{1+e^{\frac{[(2c+d)/t-A_3]}{A_4}}}+A_4 \quad (8)$$

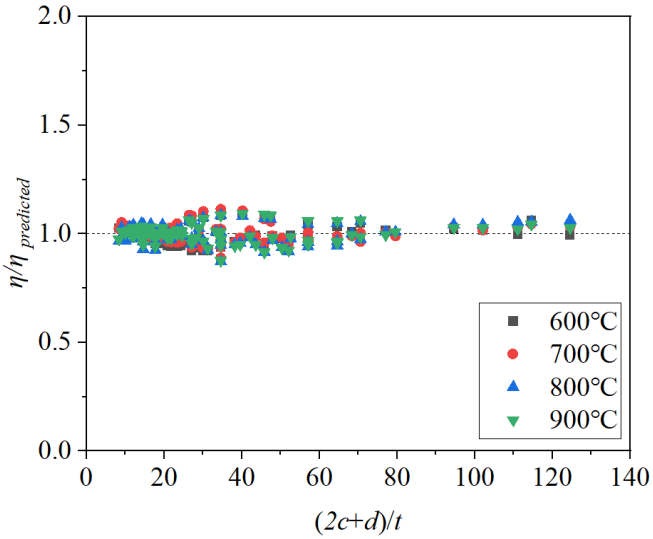

Fig. 16. Comparison in correction factor η between FE results and results from Eq. (8).

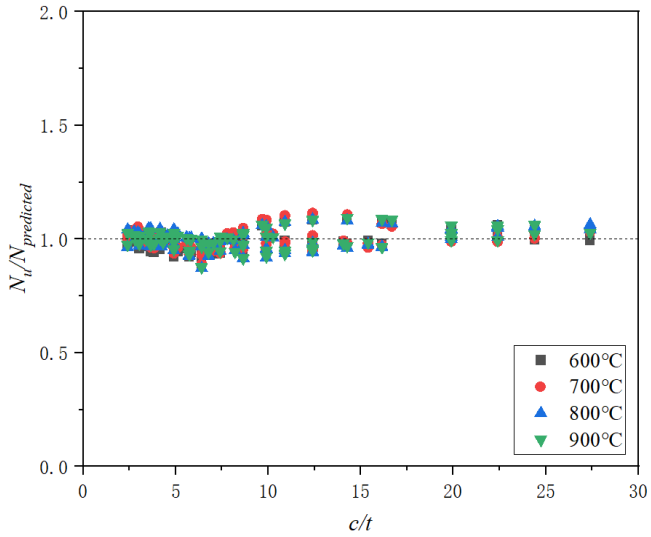

Fig. 17. Comparison in ultimate resistance between FE and predicted results.

Table 5

Coefficients in the proposed Eq. (8).

Exposure temperatures	A_1	A_2	A_3	A_4
600 °C	1.00	1.16	42.77	68.99
700 °C	0.73	0.90	39.81	7.86
800 °C	0.96	0.65	16.24	4.69
900 °C	1.08	0.78	16.46	5.88

Table 6

Quantitatively discussion on $\eta/\eta_{predicted}$.

Exposure temperatures	600 °C	700 °C	800 °C	900 °C
Mean	0.99	1.00	1.00	1.00
COV (Coefficient of Variation)	0.043	0.043	0.044	0.041

4.2.2. Modification proposal II

Based on the discussion in the subsection 4.1.1 of this paper, for the cold–formed Q960 UHSS channel section stub columns without fire exposure and with 600 and 700 °C exposure temperatures, the EC3 design approach [29] performed the good accuracy on the ultimate resistance. However, when c/t was smaller than 10.00, the accuracy of the EC3 design approach [29] on the ultimate resistance of the cold–formed Q960 UHSS channel section stub columns after 800 and 900 °C exposure temperatures was significantly reduced, which was caused by the strain hardening of the Q960 UHSS. With increment in $(2c+d)/t$, the cross–section became slenderer. The buckling weakened the beneficial effects of strain hardening on the load–bearing capacity of the cold–formed Q960 UHSS channel section stub columns after exposure to 800 and 900 °C. Then, with the reduction in beneficial effects of strain hardening, the accuracy of EC3 design approach [29] on the N_u was improved. The ratio N_u/N_{EC3} gradually approached 1. Based on the graphic evaluation, there were negative relations between the N_u/N_{EC3} and $(2c+d)/t$. To clarify the above negative relations, the variation trends of the N_u/N_{EC3} with different $(2c+d)/t$ were shown in Fig. 18. The negative nonlinear relations between N_u/N_{EC3} and $(2c+d)/t$ could be quantified trough the quadratic polynomial Eq. (9). The coefficients in the proposed Eq. (9) were determined based on the numerical results, which were shown in Table 7. The comparison in Fig. 18 stated

627 the effectiveness of the proposed Eq. (9). When the exposure temperatures were at 800
628 and 900 °C and the $(2c+d)/t$ was less than 40, the ultimate resistance of cold–formed
629 Q960 UHSS channel section stub columns could be quantified by ξN_{EC3}. The
630 comparisons between the numerical results and the results from modified EC3 design
631 approach were shown in Fig. 19. Based on the modification proposed in this study, the
632 accuracy of EC3 design approach [29] on the ultimate resistance of cold–formed Q960
633 UHSS channel section stub columns with different exposure temperature was improved.

$$\xi = B_1 \left(\frac{2c+d}{t}\right)^2 + B_2 \left(\frac{2c+d}{t}\right) + B_3 \qquad (9)$$

634

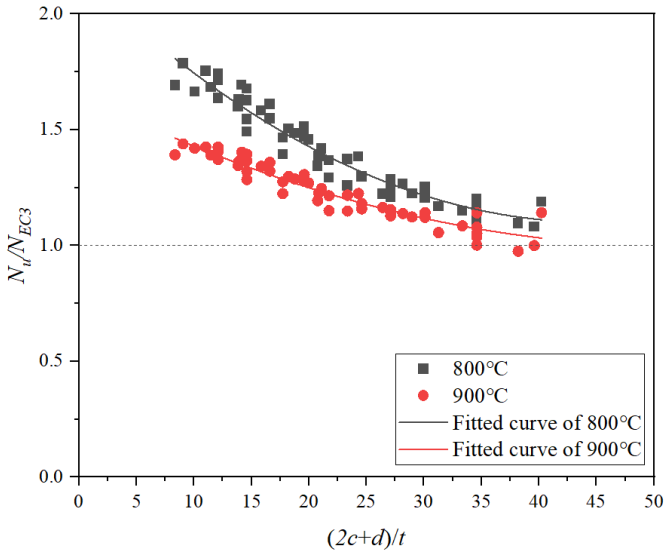

635

636 Fig. 18. Relations between N_u/N_{EC3} and $(2c+d)/t$

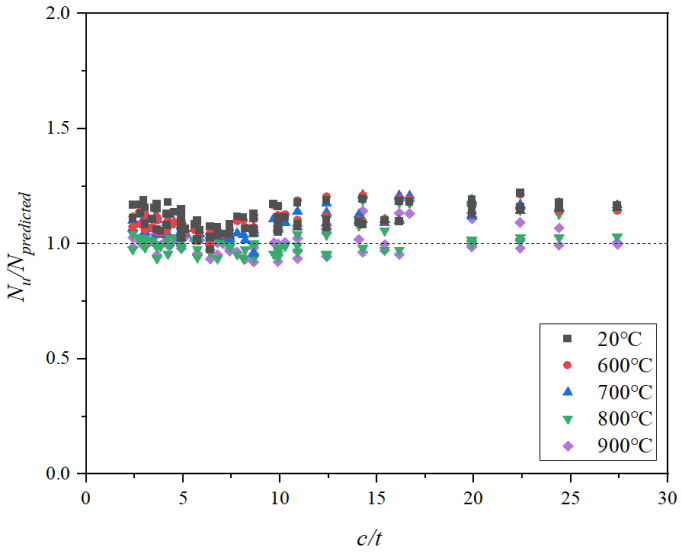

637

638 Fig. 19. Comparison between numerical results and the results from modified EC3

639 design approach.

640 Table 7

641 Coefficients in the proposed Eq. (9).

Exposure temperatures	B_1	B_2	B_3
800 °C	5.32E-04	-0.0477	2.17
900 °C	2.38E-04	-0.0251	1.65

642

643 # 5. Conclusions

644 A series of FE analyses were conducted to investigate the residual resistant performance
645 of the cold–formed Q960 UHSS channel section stub columns after fire exposure. The
646 main conclusions were listed as follows:

647 1. The numerical modelling method proposed in this study was validated by the existing
648 experimental results of the cold–formed EN 1.4420 austenitic stainless steel, S690 HSS
649 and S960 UHSS channel section stub columns under room temperature and the hot-
650 rolled EN 1.4301 austenitic stainless steel channel section stub columns after exposure
651 to fire. Numerical results stated the accuracy on the ultimate resistance, load–end
652 shortening curve and failure mode. A parametric study consisting of 410 numerical

models was conducted, where the different geometric dimensions (B_w, B_f and t) and exposure temperatures were considered.

2. Based on the parametric study results, the effects of exposure temperature on the load–end shortening curve and failure mode of the cold–formed Q960 UHSS channel section stub columns were investigated. The geometric dimensions of cold–formed Q960 UHSS channel section stub columns changed the effects of exposure temperature on the load–end shortening curves. For the load–end shortening curves of the stub columns with Class 1 to 3 (stocky) cross–sections, there was a noteworthy increment in load after the initial rising segment, because of the beneficial effects of the strain hardening in monotonic stress–strain curves. The stub columns with slender cross–section were more prone to buckling.

3. Effects of the exposure temperature and the geometric dimension on the ultimate resistance of the cold–formed Q960 UHSS channel section stub columns after fire exposure were also studied. The effects of exposure temperature on the ultimate resistance changed, with the increment in $(2c+d)/t$. The ultimate resistances obtained from the numerical analyses were used to assess the slenderness limit of Class 3 in EC3 [29]. For the condition at 600 °C exposure temperature and without fire exposure, the slenderness limit of Class 3 in EC3 [29] could be used on the cold–formed Q960 UHSS channel section stub columns. However, when the exposure temperatures were at 700, 800 and 900 °C, the slenderness limit of Class 3 in EC3 became unsuitable. The accuracy of design approaches in EN 1993-1-12 [29], AISI S100 [30], AS/NZS 4600 [31] and DSM was assessed.

4. The ultimate resistance of the cold–formed Q960 UHSS channel section stub columns without fire exposure could be accurately predicted by the design approaches in EN 1993-1-12 [29], AISI S100 [30] and AS/NZS 4600 [31]. When the exposure temperatures were at 800 and 900 °C, there were noteworthy differences between the FE results and the results calculated from EN 1993-1-12 [29], AISI S100 [30], AS/NZS 4600 [31] and DSM. The modification methods considering effects of the exposure

temperature and the geometric dimension were proposed for the design approach in EN 1993-1-12 [29] to quantify the residual ultimate resistance of the cold–formed Q960 UHSS channel section stub columns after different exposure temperatures.

This study only revealed on the residual ultimate resistance of the cold–formed Q960 UHSS channel section stub columns after fire exposure. To achieve a comprehensive evaluation on the residual resistant performance of cold–formed Q960 UHSS structures after fire, more investigations should be conducted on cold–formed UHSS sections with different steel strength grades, cross–section shapes, loading conditions, and boundary conditions.

CRediT authorship contribution statement

Xuanyi Xue: Conceptualization, Investigation, Validation, Writing –original draft, Writing – review & editing. **Tak-Ming Chan**: Conceptu- alization, Resources, Supervision, Writing – review & editing. **Ben Young**: Conceptualization, Resources, Supervision, Writing – review & editing.

Declaration of Competing Interest

The authors declare that they have no known competing financial interests or personal relationships that could have appeared to influence the work reported in this paper

Data availability

Data will be made available on request.

Acknowledgement

The support from the Chinese Engineering Research Centre for Steel Construction (Hong Kong Branch) at The Hong Kong Polytechnic University is gratefully appreciated.

References

[1] G.Q. Li, H. Lyu, C. Zhang, Post-fire mechanical properties of high strength Q690 structural steel, J. Constr. Steel Res. 132 (2017) 108–116. https://doi.org/10.1016/j.jcsr.2016.12.027.

[2] F. Wang, O. Zhao, B. Young, Testing and numerical modelling of S960 ultra-high strength steel angle and channel section stub columns, Eng. Struct. 204 (2020) 109902. https://doi.org/10.1016/j.engstruct.2019.109902.

[3] L. Zhang, F. Wang, Y. Liang, O. Zhao, Press-braked S690 high strength steel equal-leg angle and plain channel section stub columns: Testing, numerical simulation and design, Eng. Struct. 201 (2019) 109764. https://doi.org/10.1016/j.engstruct.2019.109764.

[4] Y. Xiao, X. Xue, F.F. Sun, G.Q. Li, Postbuckling shear capacity of high-strength steel plate girders, J. Constr. Steel Res. 150 (2018) 475–490. https://doi.org/10.1016/j.jcsr.2018.08.032.

[5] Y. Xiao, X. Xue, F.F. Sun, G.Q. Li, Intermediate transverse stiffener requirements of high-strength steel plate girders considering postbuckling capacity, Eng. Struct. 196 (2019) 109289. https://doi.org/10.1016/j.engstruct.2019.109289.

[6] G. Shi, W.J. Zhou, C.C. Lin, Experimental Investigation on the Local Buckling Behavior of 960 MPa High Strength Steel Welded Section Stub Columns, Adv. Struct. Eng. 18 (2015) 423–437.

[7] J.-L. Ma, T.-M. Chan, B. Young, Experimental Investigation on Stub-Column Behavior of Cold-Formed High-Strength Steel Tubular Sections, J. Struct. Eng. 142 (2016). https://doi.org/10.1061/(asce)st.1943-541x.0001456.

[8] D. Li, Z. Huang, B. Uy, H.T. Thai, C. Hou, Slenderness limits for fabricated S960 ultra-high-strength steel and composite columns, J. Constr. Steel Res. 159 (2019) 109–121. https://doi.org/10.1016/j.jcsr.2019.04.025.

[9] Y. Cai, F. Zhou, L. Wang, B. Young, Design of lean duplex stainless steel tubular sections subjected to concentrated end bearing loads at elevated temperatures, Thin-Walled Struct. 160 (2021) 107298. https://doi.org/10.1016/j.tws.2020.107298.

[10] J. Chen, B. Young, Design of high strength steel columns at elevated temperatures, J. Constr.

Steel Res. 64 (2008) 689–703. https://doi.org/10.1016/j.jcsr.2007.09.004.

[11] H. Li, K. Zhan, B. Young, Web crippling design of cold-formed high strength steel SHS and RHS at elevated temperatures, Thin-Walled Struct. 180 (2022) 109716. https://doi.org/10.1016/j.tws.2022.109716.

[12] J. Hua, X. Xue, Q. Huang, Y. Shi, W. Deng, Post-fire performance of high-strength steel plate girders developing post-buckling capacity, J. Build. Eng. 52 (2022) 104442. https://doi.org/10.1016/j.jobe.2022.104442.

[13] Y. Shi, J. Wang, X. Zhou, X. Xue, Post – fire properties of stainless – clad bimetallic steel produced by explosive welding process, J. Constr. Steel Res. 201 (2023) 107690. https://doi.org/10.1016/j.jcsr.2022.107690.

[14] J. Hua, F. Wang, X. Xue, Y. Sun, Y. Gao, Post-fire ultra-low cycle fatigue properties of high-strength steel via different cooling methods, Thin-Walled Struct. 183 (2023) 110406. https://doi.org/10.1016/j.tws.2022.110406.

[15] J. Hua, Z. Yang, F. Wang, X. Xue, N. Wang, L. Huang, Relation between the metallographic structure and mechanical properties of a bimetallic steel bar after fire, J. Mater. Civ. Eng. 34 (2022) 04022193. https://doi.org/10.1061/(ASCE)MT.1943-5533.0004351.

[16] F. Azhari, A.H. Apon, A. Heidarpour, X. Zhao, C.R. Hutchinson, Mechanical response of ultra-high strength (Grade 1200) steel under extreme cooling conditions, Constr. Build. Mater. 175 (2018) 790–803. https://doi.org/10.1016/j.conbuildmat.2018.04.191.

[17] M.T. Chen, M. Pandey, B. Young, Mechanical properties of cold-formed steel semi-oval hollow sections after exposure to ISO-834 fire, Thin-Walled Struct. 167 (2021) 108202. https://doi.org/10.1016/j.tws.2021.108202.

[18] M. Pandey, B. Young, Post-fire mechanical response of high strength steels, Thin-Walled Struct. 164 (2021) 107606. https://doi.org/10.1016/j.tws.2021.107606.

[19] H.T. Li, B. Young, Residual mechanical properties of high strength steels after exposure to fire, J. Constr. Steel Res. 148 (2018) 562–571. https://doi.org/10.1016/j.jcsr.2018.05.028.

[20] X. Qiang, F.S.K. Bijlaard, H. Kolstein, Post-fire performance of very high strength steel S960, J. Constr. Steel Res. 80 (2013) 235–242. https://doi.org/10.1016/j.jcsr.2012.09.002.

[21] X. Xue, Y. Shi, X. Zhou, J. Wang, Y. Xu, Experimental study on the properties of Q960 ultra–high–strength steel after fire exposure, Structures. 47 (2023) 2081–2098. https://doi.org/10.1016/j.istruc.2022.12.034.

[22] L.X. Song, G.Q. Li, Y.C. Wang, Experimental study on the effects of whole heating cycle on post-fire behavior of restrained high strength structural steel columns, J. Build. Eng. 70 (2023) 106385. https://doi.org/10.1016/j.jobe.2023.106385.

[23] A. Su, K. Jiang, Y. Wang, O. Zhao, Experimental and numerical investigations into S960 ultra-high strength steel welded I-section stub columns after exposure to elevated temperatures, Thin-Walled Struct. 183 (2023) 110349. https://doi.org/10.1016/j.tws.2022.110349.

[24] M. Sagiroglu, Experimental evaluation of the post-fire behavior of steel T-component in the beam-to-column connection, Fire Saf. J. 96 (2018) 153–164. https://doi.org/10.1016/j.firesaf.2018.01.007.

[25] M. Pandey, B. Young, Post-fire behaviour of cold-formed high strength steel tubular T- and X-joints, J. Constr. Steel Res. 186 (2021) 106859. https://doi.org/10.1016/j.jcsr.2021.106859.

[26] Y.H. Cho, L.H. Teh, B. Young, A. Ahmed, Net section tension strength of bolted connections in ultra-high strength sheet steel during and after fire, J. Constr. Steel Res. 172 (2020) 106237. https://doi.org/10.1016/j.jcsr.2020.106237.

[27] X. Xue, Y. Shi, X. Zhou, J. Wang, Y. Xu, Experimental study on the properties of Q960 ultra–high–strength steel after fire exposure, Structures. 47 (2023) 2081–2098. https://doi.org/https://doi.org/10.1016/j.istruc.2022.12.034.

[28] Y. Shi, J. Wang, X. Zhou, X. Xue, Y. Li, Post-fire mechanical properties of Q960 cold-formed thick-walled ultra-high-strength steel, Fire Technol. (2024) 1–37. https://doi.org/10.1007/s10694-024-01555-3.

[29] EN 1993-1-12. Eurocode 3: Design of steel structures-Part 1-12: Additional rules for the extension of EN 1993 up to steel grades S 700, Brusseles: European Committee for Standardization, 2007.

[30] AISI S100. North American specification for the design of cold-formed steel structural members, American Iron and Steel Institute, 2016.

[31] AS/NZS 4600. Cold-formed steel structures, Australian/New Zealand Standard, Sydney: AS/NZS 4600, 2018.

[32] X. Zhou, X. Xue, Y. Shi, J. Xu, Post-fire mechanical properties of Q620 high-strength steel with different cooling methods, J. Constr. Steel Res. 180 (2021) 106608. https://doi.org/10.1016/j.jcsr.2021.106608.

[33] W. Wang, Y. Zhang, X. Li, Experimental Study on Mechanical Properties of High Strength Q960 Steel after High Temperature, Jianzhu Cailiao Xuebao/Journal Build. Mater. 25 (2022) 102–110. https://doi.org/10.3969/j.issn.1007-9629.2022.01.015.

[34] ABAQUS. ABAQUS/Standard user's Manual Volumes I-III and ABAQUS CAE Manual. Version 2020.Hibbitt, Karlsson & Sorensen, Inc:Pawtucket, USA, 2020.

[35] Y. Huang, B. Young, Finite element analysis of cold-formed lean duplex stainless steel columns at elevated temperatures, Thin-Walled Struct. 143 (2019) 106203. https://doi.org/10.1016/j.tws.2019.106203.

[36] L. Zhang, K.H. Tan, O. Zhao, Local stability of press-braked stainless steel angle and channel sections: Testing, numerical modelling and design analysis, Eng. Struct. 203 (2020) 109869. https://doi.org/10.1016/j.engstruct.2019.109869.

[37] X. Lan, S. Li, O. Zhao, Local buckling of hot-rolled stainless steel channel section stub columns after exposure to fire, J. Constr. Steel Res. 187 (2021) 106950. https://doi.org/10.1016/j.jcsr.2021.106950.

[38] EN 1993-1-1. Eurocode 3: Design of Steel Structures-Part 1-1: General rules and rules for buildings, Brusseles: European Committee for Standardization, 2005.

[39] Y. Huang, J. Chen, Y. He, B. Young, Design of cold-formed stainless steel RHS and SHS beam–columns at elevated temperatures, Thin-Walled Struct. 165 (2021) 107960. https://doi.org/10.1016/j.tws.2021.107960.

[40] B.W. Schafer, Review: The Direct Strength Method of cold-formed steel member design, J. Constr. Steel Res. 64 (2008) 766–778. https://doi.org/10.1016/j.jcsr.2008.01.022.

[41] Z. Wang, C. Ma, M. Li, Q. Han, H.T. Li, D. Zhao, Mechanical properties of 7A04-T6 high strength structural aluminium alloy at elevated temperatures and after cooling down, Thin-

Walled Struct. 180 (2022) 109930. https://doi.org/10.1016/j.tws.2022.109930.

[42] Y. Huang, B. Young, Mechanical properties of lean duplex stainless steel at post-fire condition, Thin-Walled Struct. 130 (2018) 564–576. https://doi.org/10.1016/j.tws.2018.06.018.

[43] X. Qiang, F.S.K. Bijlaard, H. Kolstein, Post-fire mechanical properties of high strength structural steels S460 and S690, Eng. Struct. 35 (2012) 1–10. https://doi.org/10.1016/j.engstruct.2011.11.005.